**Fig. 4.** The UV spectra of different SnO$_2$ materials. (1) Micrometer-sized crystals obtained from oxidation of tin at 1000°C; (2) H-gel fired at 500°C for 1 hour; (3) U-gel fired at 500°C for 1 hour; and (4) U-gel fired at 800°C for 1 hour.

Fig. 5. The response curves of CO sensors made of Pd-impregnated U-SnO$_2$ (dashed line) and H-SnO$_2$ (solid line) films at 20°C.

and result in a lower (red-shifted) absorption edge. Furthermore, after firing above 400°C, the red-shift decreases as defect density decreases. Although the H-grains fired at 500°C (MCS of ~20 Å) are 10 times smaller, they actually have a higher absorption edge energy (curve 2), that is, they have fewer defects than the U-grains (curve 3). Additional firing of the U-gel at 800°C for 1 hour gave the same UV absorption profile (curve 4) as that of the H-gel fired at 500°C, but its MCS increased to ~450 Å and its SSA dropped to 10 m^2/g.

Firing of the H-TiO$_2$ gels at 500°C produces anatase crystallites with an MCS of 50 Å, as compared with 150 Å for the U-gel (Table 1). Under the same conditions, ZrO$_2$ gel crystallizes into the metastable tetragonal, rather than monolithic, crystallites with an MCS of 15 Å. For both oxides, the H-gels have a much greater SSA (Table 1) and smaller pore sizes (Fig. 1) than their U-gel counterparts.

Maintaining smaller crystal sizes can improve device performance. For example, in the following chemical-sensor application, Pd-containing SnO$_2$ films were prepared by first spin-coating the hydrous SnO$_2$ precipitate containing 1 mole percent Pd^{2+} onto silica substrates. The films, either treated or untreated with HMDS, were fired at 350°C for 1 hour. The fired films were subsequently exposed to atmospheres repeatedly switched between air and CO (500 ppm)–air mixture, and the resistances, R_{Air} and R_{CO}, respectively, were monitored with the four-point method. For polycrystalline conductors, grain boundaries contribute most of the resistance, especially when the intragrain defect density is low. The surface resistivity of an oxide crystal depends on the electron concentration near the surface, which in turn is affected by the nature of the chemisorbed species. Theoretically, the smaller the crystal size, the greater the sensitivity of overall resistance to the surrounding atmosphere.

The U-film showed a sensitivity (R_{Air}/R_{CO}) of 1.8 at 20°C, whereas the H-film gave an R_{Air}/R_{CO} ratio of ~90, a 50-fold increase (Fig. 5). The H-film is, in fact, an extremely
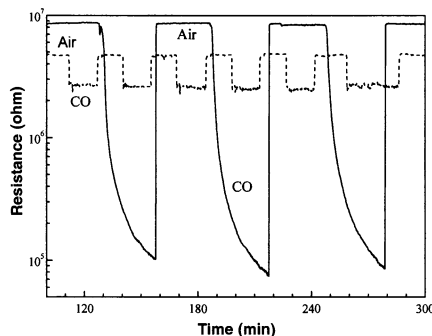
sensitive SnO$_2$-based CO sensor at room temperature, as typically the sensitivity of such films is no greater than 5.0 (12).

References and Notes
1. C. E. Brinker and G. W. Scherer, *Sol-Gel Sci.* (Academic Press, San Diego, CA, 1990), pp. 515–738.
2. N. L. Wu, L. F. Wu, I. A. Rusakova, A. Hamed, A. P. Litvinchuk, *J. Am. Ceram. Soc.* **82**, 67 (1999).
3. D. M. Antonelli and J. Y. Ying, *Angew. Chem. Int. Ed.* *Engl.* **34**, 2014 (1995); L. Qi, J. Ma, H. Cheng, Z. Zhao, *Langmuir* **14**, 2579 (1998).
4. W. M. H. Sachtler and Y. Y. Huang, U.S. Patent 5,786,294.
5. K. Takahata, in *Chemical Sensor Technology*, T. Seiyama, Ed. (Elsevier, Amsterdam, 1988), vols. 1 and 2.
6. A. J. Burggraaf and K. Keizer, in *Inorganic Membranes: Synthesis, Characterization and Applications*, R. R. Bhave, Ed. (Van Nostrand Reinhold, New York, 1991), chap. 2.
7. Japanese Patent 2-1104.
8. Experiments with trimethylchlorosilane (TMCS) have also been performed and have given similar results. However, HMDS is less corrosive and much easier to handle than TMCS.
9. C. M. Jin, J. D. Luttmer, D. M. Smith, T. A. Ramos, *MRS Bull.* **22** (no. 10), 39 (1997).
10. N. L. Wu, L. F. Wu, Y. C. Yang, S. J. Huang, *J. Mater. Res.* **11**, 813 (1996).
11. *Infrared Structural Correlation Tables and Data Cards*, R. G. J. Miller and H. Willis, Eds. (Heyden, London, 1969), tables 9-A2a and 9-x3.
12. P. Bonzi *et al.*, *J. Mater. Res.* **9**, 1250 (1994); A. Nakajima, *J. Mater. Sci. Lett.* **12**, 1778 (1993); G. S. V. Coles, K. J. Gallagher, J. Watson, U. K. Patent GB 2177215.
13. Supported by the National Science Council of the Republic of China under contract NSC86-2113-M-002-006. TEM work was supported by the State of Texas through funding for the Texas Center for Superconductivity at the University of Houston.

Asteroidal Water Within Fluid Inclusion–Bearing Halite in an H5 Chondrite, Monahans (1998)

Michael E. Zolensky,[1]* **Robert J. Bodnar,**[2] **Everett K. Gibson Jr.,**[1] **Laurence E. Nyquist,**[1] **Young Reese,**[3] **Chi-Yu Shih,**[3] **Henry Wiesmann**[3]

Crystals of halite and sylvite within the Monahans (1998) H5 chondrite contain aqueous fluid inclusions. The fluids are dominantly sodium chloride–potassium chloride brines, but they also contain divalent cations such as iron, magnesium, or calcium. Two possible origins for the brines are indigenous fluids flowing within the asteroid and exogenous fluids delivered into the asteroid surface from a salt-containing icy object.

Over the past three decades, we have become increasingly aware of the fundamental importance of water and aqueous alteration on primitive solar system bodies. Some carbonaceous and ordinary chondrites, long touted as primordial material relatively unchanged since formation, have been altered by interactions with liquid water within the first 10 million years after formation of their parent asteroids (1). Nevertheless, we do not know the location and timing of the aqueous alteration or the nature of the aqueous fluid itself.

Workers have attempted to model and understand this aqueous process through analysis of hydrated minerals present in the meteorites and through computer simulations of the alteration process (2). A major impediment to our understanding of aqueous alteration has been the absence of actual samples of aqueous fluids in meteorites. Here, we report the discovery and characterization of aqueous fluid inclusions in an ordinary chondrite.

The Monahans (1998) (hereafter Monahans) ordinary chondrite fell on 22 March 1998 in Monahans, Texas. The fall was witnessed by seven boys, and the first of two stones was recovered immediately. This first stone was carried to the Johnson Space Center and broken open in a filtered-air, clean-room facility <48 hours after the fall, effectively eliminating the opportunity for aqueous or other contamination
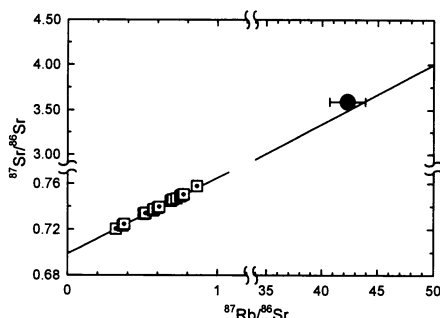
[1]Mail Code SN2, NASA Johnson Space Center, Houston, TX 77058, USA. [2]Department of Geological Sciences, Virginia Tech, Blacksburg, VA 24061, USA. [3]Lockheed Martin Space Operations Company, Houston, TX 77058, USA.

*To whom correspondence should be addressed.

of the interior of the meteorite (*3*). The meteorite is a regolith breccia consisting of light and dark clasts set within a gray matrix; the hue is controlled by the shock level. The light lithology has witnessed shock level S2 (5 to 10 GPa), the gray lithology has witnessed S3 (10 to 15 GPa), and the dark lithology has witnessed S4 (15 to 30 GPa) (*4*). All lithologies are H5, which indicates moderate thermal metamorphism (*5*). After breaking open the first sample, we noted that the gray matrix contains locally abundant aggregates of purple halite (NaCl) crystals, measuring up to 3 mm in diameter. To the best of our knowledge, megascopic halite has not been previously seen in any extraterrestrial sample, although microscopic halite has been reported in several meteorites (*6–8*). Backscattered electron imaging of Monahans reveals that crystals of sylvite (KCl) are present within the halite crystals, similar to their occurrence in terrestrial evaporites (*9*). The purple color of the halite may be caused by exposure to solar and galactic cosmic rays, exposure to beta-decaying ^{40}K in the sylvite (*9, 10*), or a combination of these effects. The presence of halite and sylvite only within the gray matrix indicates that the halite may have formed at the surface of the asteroid, before final aggregation of the meteorite. However, its deposition probably postdates the most severe thermal metamorphism and shock, because halite is a brittle material that could not have survived these processes.

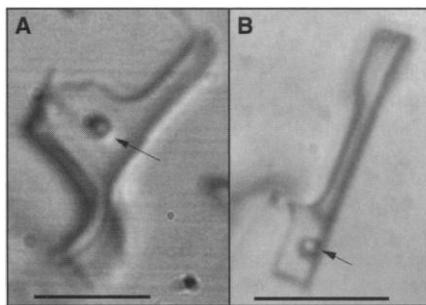The three lithologies of Monahans were an-

alyzed separately for noble gases (*11*), which revealed that Monahans is a regolith breccia. Relative amounts of He, ^{20}Ne, and ^{36}Ar in the gray matrix and dark clasts indicate a major contribution of solar wind–implanted gases (*11*). The gray matrix lithology contains the highest concentration of solar wind–implanted gas (at standard temperature and pressure, cosmogenic ^{21}Ne and ^{38}Ar is 3.0^{-8} and 3.4×10^{-9} to 4.2×10^{-9} cm^3 g^{-1}, respectively) (*11*), indicating that it was pre-irradiated for a few million years on the surface of its parent asteroid during the time of the halite deposition and before its ejection as a meteorite.

One milligram of Monahans halite with sylvite was used for Rb/Sr analysis by mass spectrometry (*12*). This sample contains 3.75 ± 0.08 parts per million (ppm) of Rb and 0.257 ± 0.006 ppm of Sr, leading to the following ratios: $^{87}Rb/^{86}Sr = 43.3 \pm 1.6$ and $^{87}Sr/^{86}Sr = 3.59 \pm 0.07$. With a ^{87}Rb decay constant of 0.01402 giga-annum^{-1} (Ga^{-1}) (*12*) and an initial ratio of $^{87}Sr/^{86}Sr = 0.698972$ (*13*), the calculated Rb-Sr model age for the halite is 4.7 ± 0.2 Ga. The bulk H-group chondrites define an age of 4.58 ± 0.04 Ga (*14*), which is within the error limits of our reference isochron of 4.56 Ga (Fig. 1). Because the isotopic composition of Sr in the halite and sylvite is very radiogenic, the model age is considered to be the formation age of the halite; it formed early in the history of the Monahans parent asteroid.
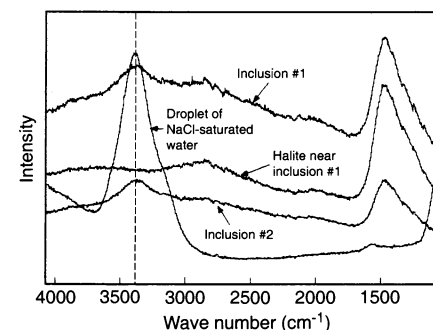
Fluid inclusions are microsamples of fluid that are trapped as isolated inclusions in the crystal during growth (primary inclusions) or at some later time along a healed fracture in the mineral (secondary inclusions), forming planes (*15*). Primary and secondary fluid inclusions are found in Monahans halite, with secondary inclusions being predominate (~80%). The presence of secondary inclusions in the halite indicates that aqueous fluids were locally present after halite deposition, suggesting that aqueous activity could have been episodic.

The inclusions range up to 15 μm in their longest dimension (Fig. 2). At room temperature, a few of the inclusions (~25%) contain bubbles that are in constant motion, indicat-

ing that the inclusions contain a low-viscosity liquid and vapor. The remaining inclusions contain only a single liquid phase. During the cooling of 10 randomly selected inclusions under a microscope, the inclusions solidified (froze) at $-45°$ to $-50°C$. Thus, the liquid in the inclusions cannot be carbon dioxide, because solid and vapor carbon dioxide cannot coexist at any temperature above the triple point of carbon dioxide, which is $-56.6°C$. Moreover, the vapor bubble appeared to shrink and in some cases disappear during freezing, consistent with the interpretation that the inclusions contain an aqueous solution (if the inclusions were pure carbon dioxide, the bubble would become larger when liquid carbon dioxide was frozen to form solid carbon dioxide). When the frozen inclusions were heated, melting was initially observed at about $-35°$ to $-40°C$, indicating that the inclusions may contain divalent cations such as Fe^{2+}, Ca^{2+}, or Mg^{2+}, in addition to Na$^+$ and K$^+$ (*16*). Given the environment of formation (*1*), dissolved Fe and Ca are the most likely cause of the lowered first melting temperatures, unlike in terrestrial evaporite environments, in which Ca and Mg cause a reduction in the melting temperatures. The final ice-melting temperature was difficult to determine with any degree of accuracy. The halite sample containing the fluid inclusions described here was not polished (it was simply broken out of the meteorite with a needle) and had been carbon coated for earlier electron microprobe analysis. As a result, the optics on the petrographic microscope were poor. This, combined with the small size of the inclusions and the layer of glass between the microscope objective lens and the sample during cooling, made observation of phase changes difficult. It is estimated that final ice melting occurred at or

Fig. 1. $^{87}Rb/^{86}Sr$ and $^{87}Sr/^{86}Sr$ systematics for the Monahans halite and bulk H-group chondrites. The reference 4.56-Ga isochron is calculated for an initial ratio of $^{87}Sr/^{86}Sr = 0.698972$, determined for angrite LEW86010 (*13*) and a ^{87}Rb decay constant of 0.01402 Ga^{-1} (*14*). Monahans halite is shown as a shaded circle; error bars indicate analytical uncertainties. Data for bulk H-group chondrites (*14*) are plotted as open squares, and the diagonal line is an isochron fitted to the data for H-group chondrites. Strontium in the Monahans halite is very radiogenic; thus, the halite age is insensitive to uncertainties in the initial $^{87}Sr/^{86}Sr$ ratio. The model age of 4.7 ± 0.2 Ga calculated for an initial ratio of $^{87}Sr/^{86}Sr = 0.69876 \pm 0.00040$, the average for H-group chondrites (*14*), is the same as that calculated for the angrite initial $^{87}Sr/^{86}Sr$ ratio, assumed to be representative of the early solar system.

Fig. 2. Transmitted light images of fluid inclusions in Monahans halite. (**A** and **B**) Primary inclusions, each containing a liquid and a small bubble (indicated by arrows). Scale bars, 5 μm.

Fig. 3. Raman microprobe spectra of Monahans fluid inclusions, halite, and NaCl-saturated water. The two spectra of fluid inclusions in Monahans halite (inclusions 1 and 2) show a broad peak at ~3400 cm^{-1} (indicated by vertical dashed line). A spectrum of Monahans halite near inclusion 1 lacks the 3400 cm^{-1} peak. A spectrum of a droplet of NaCl-saturated water (with a peak at 3400 cm^{-1}) is shown for comparison; the peak at ~1000 cm^{-1} in this spectrum is from the glass slide.

slightly below $-20°C$, because at this temperature the vapor bubble moved freely within the inclusions. Below this temperature, the bubble was generally pinned into one place or moved only in a restricted region of the inclusion, presumably because of the presence of ice (or hydrate phases) that could not be discerned optically.

The presence of water in the inclusions was confirmed by Raman microprobe analysis (17). Raman spectra of inclusions in Monahans halite show a peak at ~3400 cm^{-1}, which is diagnostic of aqueous salt solutions (Fig. 3). Pure water gives a broad peak that is skewed to lower wave numbers. With the addition of salt, the peak becomes more symmetrical and narrower (18), as shown by the spectrum for a droplet of NaCl-saturated water collected at the same conditions used for the two inclusions in halite. The Raman spectrum of an area of the halite away from inclusions does not show a peak in the region of 3000 to 4000 cm^{-1} (Fig. 3), indicating that the species responsible for the peak occurs in the inclusions but not in the halite.

The minimum temperature of formation of a given fluid inclusion may be estimated on the basis of the relative size of the vapor bubble in the inclusion at room temperature. Thus, a pure water inclusion with a homogenization temperature of $374°C$ would contain 69% by volume vapor at room temperature, whereas a pure water inclusion with a homogenization temperature of $200°C$ would contain $\sim15\%$ by volume vapor at room temperature. Fluid inclusions with homogenization temperatures $<100°C$ often fail to nucleate a vapor bubble when cooled to room temperature and remain as single-phase liquid inclusions that are metastable (15). The rarity of vapor bubbles in fluid inclusions in Monahans halite (we only observed 11 bubbles in ~40 inclusions) suggests a low formation temperature ($<100°C$), assuming that the formation pressure was low (a few tens of bars at most). The bubbles that are present only occupy ~5 to 10% by volume of the inclusions and may have resulted from freeze stretching of the inclusions during space exposure (19). The vapor bubbles represent the water vapor in equilibrium with the aqueous solution at room temperature and, as such, are essentially a poor vacuum with a pressure of ~0.03 bars. No other aqueous fluids, such as CO_2, N_2, or CH_4, were detected during Raman analysis of the inclusions. Detection limits for these species are generally in the range of 1 mole percent in fluid inclusions, indicating that if the gases are present, their concentrations are low.

There have been numerous reports of liquid inclusions in meteorites (20). One of the more widely known studies of fluid inclusions in meteorites, and the one that led to reports of fluid inclusions in meteorites being viewed with skepticism over the past 15 years, was that by Warner et al. (21). In that study, the authors reported the presence of two-phase liquid-vapor inclusions in silicate minerals in diogenite ALHA 77256. The interest in fluid inclusions generated in the planetary science community by this report was short-lived, however, as later investigation of the same samples showed that the inclusions were artifacts from specimen preparation fluids (22). Observations of fluid inclusions within the ordinary chondrites Peetz and Jilin (23) have never been confirmed. The fluid inclusions reported here in the Monahans chondrite are a confirmation that aqueous fluid inclusions exist in some extraterrestrial samples.

Previous studies have indicated that Cl is inhomogeneously distributed in meteorites (24), with the result that the solar abundance of Cl is not well known. Halite was noticed in Monahans because of its purple color and large grain size, which permitted special sample preparation procedures to be employed, preserving the grains. It is possible that halite is commonly present in chondrites but has been overlooked. It is also possible that a considerable fraction of the ubiquitous sulfate and halide efflorescence noted on Antarctic meteorites (25) is derived from dissolution and reprecipitation of indigenous halite (and sulfides), rather than from components introduced from the ice as is commonly assumed.

The most important conclusion of this study is that an actual sample of the aqueous fluid presumably responsible for aqueous alteration of early solar system material has been identified and characterized, and this fluid is a brine. Two possible origins for the brines are (i) indigenous fluids flowing within the asteroid and (ii) exogenous fluids delivered into the asteroid surface from a salt-containing icy object, such as a comet. In either case, the inclusions provide ground truth concerning the nature of water in the early solar system.

References and Notes

1. E. DuFresne and E. Anders, Geochim. Cosmochim. Acta 26, 1085 (1962); H. Y. McSween, ibid. 51, 2469 (1987); M. E. Zolensky and H. Y. McSween, in Meteorites and the Early Solar System, J. Kerridge and M. Matthews, Eds. (Univ. of Arizona Press, Tucson, 1988), pp. 114–143; A. N. Krot, E. R. D. Scott, M. E. Zolensky, Meteoritics 30, 748 (1995).
2. M. E. Zolensky, W. L. Bourcier, J. L. Gooding, Icarus 78, 411 (1989); L. B. Browning and W. L. Bourcier, Meteorit. Planet. Sci. 33, 1213 (1998).
3. The meteorite fell on a fair day, was collected immediately, and nothing was done to introduce halite into it. If the finders had washed the meteorite in salty water and somehow introduced halite into the meteorite, that halite would be clear, not colored. Once the meteorite was in a clean laboratory, it was broken open with a hammer, and the halite was exposed. The crystals containing the fluid inclusions were removed by hand picking; no cutting or polishing of these samples was ever conducted.
4. D. Stöffler, K. Keil, E. R. D. Scott, Geochim. Cosmochim. Acta 55, 3845 (1991).
5. H5 represents a reduced (H) ordinary chondrite metamorphosed to $\sim700°$ to $800°C$ (level 5) [H. Y. McSween, D. W. G. Sears, R. T. Dodd, in Meteorites and the Early Solar System, J. Kerridge and M. Matthews, Eds. (Univ. of Arizona Press, Tucson, 1988), pp. 102–113].
6. D. Barber, Geochim. Cosmochim. Acta 45, 945 (1981).
7. J. Berkley, J. Taylor, K. Keil, Geophys. Res. Lett. 5, 1075 (1978).
8. J. L. Gooding, S. J. Wentworth, M. E. Zolensky, Meteoritics 26, 135 (1991); J. C. Bridges and M. M. Grady, Lunar Planet. Sci. XXIX (1998) [CD-ROM].
9. L. L. Y. Chang, R. A. Howie, J. Zussman, in Non-Silicates, vol. 5B of Rock-Forming Minerals, W. A. Deer, R. A. Howie, J. Zussman, Eds. (Longman Group, London, 1996), pp. 369–378.
10. K. Nassau, The Physics and Chemistry of Color (Wiley Interscience, New York, 1983).
11. M. E. Zolensky et al., Lunar Planet. Sci. XXX (1999) [CD-ROM].
12. Monahans halite (0.9 mg) was dissolved in 1 ml of high-purity double-distilled H_2O. A small cation exchange column (0.5-ml column volume) was used to separate alkali and alkaline-earth metals, which were then spiked with a mixed ^{87}Rb-^{84}Sr spike for Rb-Sr isotopic analyses. The Rb and Sr were separated on a microcolumn containing ~150 ml of Sr-spec resin. High-precision isotopic analyses were made with a Finnigan-MAT Model 261 mass spectrometer equipped with seven Faraday cups. The $^{87}Sr/^{86}Sr$ ratio for the halite was normalized to 0.710250 for the Sr standard [L. E. Nyquist et al., Geochim. Cosmochim. Acta. 54, 2195 (1990)]. The Rb concentration for the halite was calculated with $^{85}Rb/^{87}Rb$ normalized to 2.59265 for the Rb standard as reported for National Bureau of Standards number 984 [E. L. Garner, L. A. Machlan, I. L. Barnes, Proc. Lunar Sci. Conf. 6th, 1845 (1975)].
13. L. E. Nyquist, B. Bansal, H. Weismann, C.-Y. Shih, Meteoritics 29, 872 (1994).
14. J.-F. Minster, J.-L. Birck, C. J. Allegre, Nature 300, 414 (1982).
15. E. Roedder, Fluid Inclusions (Mineralogical Society of America, Washington, DC, 1984).
16. D. W. Davis, T. K. Lowenstern, R. J. Spencer, Geochim. Cosmochim. Acta 54, 591 (1990).
17. The Raman spectra were obtained with a Dilor X-Y Raman microprobe equipped with a Lexel Model 95 argon-ion laser and an Olympus BH-1 microscope. We used a laser power of 100 mW, a counting time of 128 s, and an 80× objective. The laser spot size was ~1 to 2 µm.
18. T. P. Mernagh and A. R. Wilde, Geochim. Cosmochim. Acta 53, 765 (1989).
19. When liquid water freezes, its volume expands $\sim12\%$. Thus, if an inclusion contains a vapor bubble occupying >12 volume % of the inclusion, there is sufficient space for the ice to expand when it forms. If, however, the inclusion contains <12 volume % vapor before freezing, the ice will expand to fill the space occupied by the vapor bubble and then exert stress on the inclusion walls, which can cause them to fracture or deform plastically, thus increasing the inclusion volume. Although freeze stretching may result in incorrect homogenization temperatures of the inclusions, it does not result in a change in the inclusion composition [J. P. Lawler and M. L. Crawford, Econ. Geol. 78, 527 (1983)].
20. These reports are abstracted in a series of fluid inclusion research summary volumes: E. Roedder, Ed., Fluid Inclusion Research (Virginia Polytechnic Institute Press, Blacksburg, 1968 to present).
21. J. L. Warner et al., Proc. Lunar Planet. Sci. Conf. 13th, Part 2, J. Geophys. Res. 88 (suppl.), A731 (1983).
22. R. L. Rudnick et al., Proc. Lunar Planet. Sci. Conf. 15th, Part 2, J. Geophys. Res. 90 (suppl.), C669 (1985).
23. C. Fieni, M. Bourote-Denise, P. Pellas, J. R. L. Touret, Meteoritics 13, 460 (1978).
24. J. G. Tarter, thesis, Arizona State University, Tempe (1981).
25. M. Langenauer and U. Krähenbühl, Earth Planet. Sci. Lett. 120, 431 (1998).
26. We thank the citizens of Monahans for providing us with the meteorite for study. E. Roedder, H. McSween, and one anonymous person provided cogent reviews. Support was provided to M.E.Z., R.J.B., and L.E.N. by NASA's Cosmochemistry Program.

22 April 1999; accepted 9 July 1999